

Electronic structure and magnetic coupling in FeSbO₄: A DFT study using hybrid functionals and GGA+U methods

Ricardo Grau-Crespo,^{1,*} Furio Corà,^{2,3} Alexey A. Sokol,² Nora H. de Leeuw,^{1,3} and C. Richard A. Catlow^{2,3}¹*School of Crystallography, Birkbeck College, University of London, Malet Street, London, WC1E 7HX, United Kingdom*²*Davy Faraday Research Laboratory, The Royal Institution of Great Britain, 21 Albemarle Street, London, W1S 4BS, United Kingdom*³*Department of Chemistry, University College London, University of London, 20 Gordon Street, London, WC1H 0AJ, United Kingdom*

Kingdom

(Received 20 June 2005; revised manuscript received 12 September 2005; published 11 January 2006)

The electronic structure of the iron (III) antimony (V) oxide FeSbO₄ is investigated using the density functional theory (DFT). We have used two different approaches for the solution of the electronic problem with periodic boundary conditions: localized basis-sets calculations with a hybrid (B3LYP) density functional, and plane-wave pseudopotential calculations with the GGA+U technique, where GGA denotes the generalized gradient approximations. Standard DFT-GGA and Hartree-Fock (HF) calculations are also presented for comparison. All the calculation methods correctly yield antiferromagnetic solutions with higher stability than the ferromagnetic solution, where the analysis of the spin density shows a clear superexchange mechanism for the propagation of the antiferromagnetic correlations in the crystal. However, both the fraction of the HF exchange introduced in the functional and the U_{eff} parameter controlling the orbital-dependent correction in the DFT+U method affect critically the calculated strength of the magnetic interactions. A reasonable agreement with experiment ($J=-25$ K) is obtained for B3LYP (20% of HF exchange) and for GGA+U with $U_{eff}=4$ eV ($J_{B3LYP}=-21$ K and $J_{GGA+U}=-22$ K). Both methods also agree well as to the relative position and chemical nature of the electronic bands, showing that FeSbO₄ is a *p-d* charge-transfer semiconductor.

DOI: 10.1103/PhysRevB.73.035116

PACS number(s): 71.20.-b

I. INTRODUCTION

Iron antimonate FeSbO₄ is a model catalyst for the selective oxidation of hydrocarbons¹ and an important component of some of the industrial catalysts for these reactions, including the ammoxidation of propene to obtain acrylonitrile, which is an intermediate in the production of synthetic rubbers and acrylic fibers. In addition, FeSbO₄ has been studied as a gas sensor for the detection of liquid-petroleum gas,² and it also has a range of interesting magnetic properties arising from the ordering of the moments on the Fe³⁺ cations.^{3,4}

The FeSbO₄ structure is described in terms of a rutile-like framework with Fe and Sb cations distributed in the octahedral sites within the oxygen lattice (Fig. 1). Most experimental studies have concluded that the cation distribution is completely disordered, although some diffraction data have also been interpreted in terms of partial cationic ordering in a supercell with triple *c* parameter compared to common rutile (see Ref. 5 for a review). Some of us have recently performed a computer modeling study⁶ of the distribution of cations where we found that Fe and Sb cations show a clear preference to alternate along the *c* axis of the crystal, while these chains of alternating cations connect laterally with significant disorder in the *a-b* plane, which prevents three-dimensional long-range ordering.

According to neutron diffraction experiments,³ FeSbO₄ presents antiferromagnetic ordering in two dimensions (perpendicular to the *c* axis). In a previous computer modeling study⁷ we correctly found that the antiferromagnetic (AFM) phase is energetically more favorable than the ferromagnetic (FM) phase, and we identified the alternation of the cations

along the [001] direction as the cause of the two-dimensional extension of the magnetic coupling in this structure. We have therefore used an appropriate simulation cell for FeSbO₄ consisting of a double unit cell in the [001] direction, which allows the Fe–Sb cation alternation along the *c* axis (Fig. 2).

In the present work we investigate the electronic and magnetic properties of iron antimonate using electronic structure computer modeling techniques. Our calculations show that FeSbO₄ is a charge-transfer semiconductor material, with antiferromagnetic correlations which propagate in two dimensions via a superexchange mechanism. The present investigation of the bulk electronic properties, besides its intrinsic interest, is also important for future studies on defect formation and surfaces of this material.

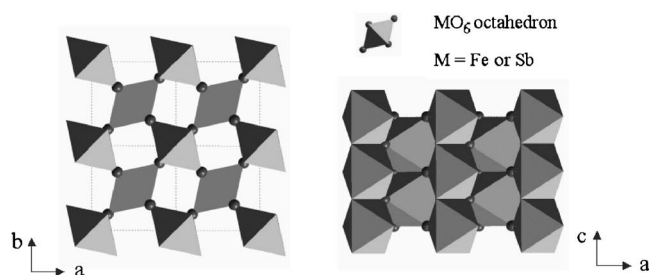


FIG. 1. Rutile-like structure of FeSbO₄. The octahedra are connected through corners in the *ab* plane and through edges in the *c* direction. According to our modeling studies (Refs. 6 and 7) Fe and Sb cations tend to alternate along the *c* axis of the crystal, while there is no clear preference for any ordered pattern in the other two directions.

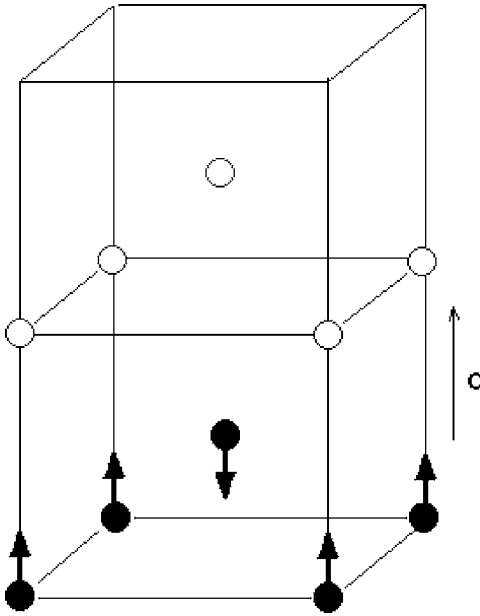


FIG. 2. Scheme of the supercell used in the calculations. Solid and open balls represent the atoms of Fe and Sb, respectively. Oxygen positions are omitted for more clarity. The arrows represent the orientation of the spin on the Fe^{3+} ions, following antiferromagnetic ordering. The orientation of the spin moments with respect to the crystal is meaningless, only their relative orientation is relevant here.

II. METHOD

We have employed computational techniques based on the density functional theory (DFT), both in the plane-wave pseudopotential formulation, using the program VASP,^{8–11} and in the all-electron formulation with localized (Gaussian) functions as the basis set, using the CRYSTAL2003 code.¹² In both cases, we have used techniques beyond the standard DFT methodology, which is based on either the local density (LDA) or the generalized gradient (GGA) approximations. The LDA and GGA are known to fail in the description of the electronic properties of early transition metal (TM) compounds, as the electron self-interaction error, always present in these formulations, becomes significant for electrons in the well-localized TM d levels.

In the CRYSTAL2003 calculations we have employed the hybrid functional B3LYP, which incorporates 20% of the Hartree-Fock (HF) exchange, and the DFT contribution is distributed between LDA and GGA parts, both for the exchange and for the correlation terms of the functional. The general performance of B3LYP and other hybrid functionals in solid state modeling has recently been discussed in detail by Cora *et al.*,¹³ showing that whenever HF and standard DFT results deviate in opposite directions from experiment, the formulation of hybrid functionals can improve the accuracy of the calculations. This improvement can be obtained for all properties that depend on the extent of electronic localization, including band gaps and magnetic coupling constants, which are of interest in FeSbO_4 . We have also performed calculations at the pure HF and GGA (BLYP) levels to compare with the B3LYP results. The BLYP functional is

TABLE I. Equilibrium cell parameters and bulk modulus for different calculation methods. c denotes parameter doubled.

Method	a (Å)	c (Å)	B (GPa)
B3LYP	4.6902	6.2488	
GGA (PW91)	4.6747	6.2342	168.7
GGA+U ^a	4.6844	6.2290	177.2
Experimental ^b	4.6433	6.1630	

^a $U_{eff}=4$ eV.

^bReference 5.

formed by the GGA exchange functional by Becke¹⁴ and the GGA correlation functional by Lee, Yang, and Parr.¹⁵ BLYP is the formal limit of a hybrid functional like B3LYP, when the HF contribution is reduced to zero.

The basis functions used in CRYSTAL2003 to expand the Kohn-Sham orbitals are atom-centered contracted Gaussian-type functions. As far as the number of Gaussian functions used for each shell are concerned, the basis sets can be described as 86 411-41 d for Fe, 976 311-631 d for Sb, and 8411-1 d for O. The basis set for iron was taken from the work by Catti, Valerio, and Dovesi¹⁶ on α - Fe_2O_3 (hematite), as the state of Fe in that structure and in iron antimonate is very similar (high-spin Fe^{3+} with octahedral coordination). The exponents and coefficients for the Sb basis were taken from the set optimized by Towler¹⁷ for the free atom, but we have removed the two most diffuse split-valence sp shells, which are not necessary for the crystalline ionic solid and may introduce numerical problems, and the exponents of the two most diffuse functions were determined variationally for the crystal structure of iron antimonate. The basis set for oxygen is the one used by Catti, Valerio, and Dovesi for hematite, but again the exponents of the two most diffuse functions were optimized for FeSbO_4 .

A full relaxation of the structure, including both the internal coordinates and the cell vectors, was performed at the B3LYP level, and the cell parameters are shown in Table I. The GGA and HF calculations were performed for the same lattice parameters as optimized at the B3LYP level, and only the atomic fractional coordinates were reoptimized for each method.

In the VASP calculations we have employed the DFT +U methodology.^{18–21} This method combines the DFT and a Hubbard Hamiltonian to account for the intra-atomic Coulomb repulsion, which is not well described in standard DFT. We use here the simple formulation by Liechtenstein, Anisimov, and Zaanen²⁰ and Dudarev *et al.*,²¹ where a single parameter U_{eff} determines an orbital-dependent correction to the DFT energy. U_{eff} is generally expressed as the difference between two parameters, the Hubbard U , which is the Coulomb-energetic cost to place two electrons at the same site, and an approximation of the Stoner exchange parameter I , which is almost constant at ~ 1 eV.²² The DFT+U correction acts by reducing the one-electron potential locally for the specified orbitals of the metal atoms (e.g., Fe d orbitals), therefore reducing the hybridization with the ligands (e.g., O atoms). The $U_{eff}=0$ case represents the DFT limit. Details of the implementation of the DFT+U method in the VASP code

can be found in the work by Rohrbach, Hofner, and Kresse on transition metal sulfides.¹⁹

The DFT solution within the DFT+U approach can be obtained either at the LDA or GGA levels, giving rise to what have been called the LDA+U and the GGA+U formulations, respectively (see Ref. 19 for a comparison between the two formulations). We have used here the GGA+U approximation with a GGA functional built from the Perdew and Zunger²³ local functional, with the spin interpolation formula of Vosko, Wilk, and Nusair²⁴ and the gradient corrections by Perdew *et al.*²⁵ It should be noted that we are referring to this functional when we talk about the GGA in the context of our plane-wave calculations, in contrast to the BLYP functional employed for the GGA calculation with localized basis sets. The interaction between the valence electrons and the core was described with the projected augmented wave method²⁶ in the implementation of Kresse and Joubert.²⁷ The number of plane waves in VASP is controlled by the cut-off energy, which in all our static calculations was $E_{cut}=400$ eV, while all the geometry relaxations were performed with an increased cut-off of 520 eV to ensure proper convergence of the stress tensor. For the optimum value of $U_{eff}=4$ eV (see discussion below) and for $U_{eff}=0$ eV (GGA limit), accurate cell parameters were also obtained by fitting the energy vs volume curve to a Murnaghan equation of state,²⁸ rather than by direct stress minimization, in order to avoid inaccuracies due to the Pulay stress.²⁹ This procedure also permits us to obtain the bulk modulus of the crystal, which is reported in Table I together with the calculated cell parameters.

Magnetic coupling constants were calculated by mapping our *ab initio* results onto the magnetic Hamiltonian:

$$H = H_0 - 2J \sum_{\{i,j\}} S_i S_j,$$

where H_0 is a constant energy, the S values for high-spin Fe^{3+} are $\pm 5/2$, and the symbol $\{i,j\}$ indicates a sum over the Fe-Fe pairs. Taking into account that there are four such pairs per unit cell, J simply becomes

$$J = \frac{E_{AFM} - E_{FM}}{100}.$$

In all cases we use the same geometry, the one corresponding to AFM equilibrium, to obtain both the FM and the AFM energy. Values are reported in the kelvin temperature scale (that is, J/k_B values, where $k_B=8.617 \times 10^{-5}$ eV/K is the Boltzmann's constant).

III. RESULTS AND DISCUSSION

A. Localized basis set calculations

Figure 3 shows the band structure and density of states calculated with the GGA, B3LYP, and HF approximations. As expected from previous studies using hybrid functionals, the band gap increases on increasing the HF component in the exchange functional. At the GGA (BLYP) level, the system has a very small band gap of around 0.2 eV, while HF predicts an insulator solution with a very large band gap of

more than 12 eV; the B3LYP predicts an intermediate band gap of around 3 eV. From experimental studies^{2,30} FeSbO_4 is known to be a semiconductor, with an activation energy of 0.75 eV for *n*-type conduction.³⁰ This value represents a lower limit for the band gap of the pure material, as it is the energy required to excite electrons from the donor levels to the conduction band. Therefore, while the electronic band gap is clearly exaggerated at the HF level, it is underestimated by the GGA calculation, and B3LYP thus provides a more realistic value. The valence space is formed by Fe-3*d* and O-2*p* states, with minor contributions from Sb-5*s* orbitals. The relative position of the respective bands changes dramatically with the approach used. In the valence bands (VB) the Fe-3*d* levels shift down with respect to the O-2*p* levels on increasing the fraction of the HF exchange: in the GGA solution, the top of the VB has largely Fe-3*d* character, although mixed with the O-2*p* levels, while in the B3LYP solution the Fe-3*d* levels are located towards the bottom of the VB, the top level being mostly O-2*p*. Finally, in the HF solution the Fe-3*d* levels are well below the O-2*p* bands. These shifts are a consequence of the self-interaction correction, accomplished via the inclusion of the HF exchange, that localizes electrons on the 3*d* orbitals, leading to a less effective overlap of the 3*d* orbitals with the O-2*p*, and the mixing of Fe/O orbitals is hence also less effective. We observe that the Fe partial density of states (DOS) in GGA covers the whole VB, while in B3LYP and even more so in the HF there are more defined peaks over a smaller energy range, which is consistent with more localized electronic states on the Fe site. However, it is worth noting that the presence of Fe and O states at the same energy does not necessarily imply Fe-O covalence; they can just overlap in the same energy range.

We also note some variations in the conduction band (CB). In GGA, the bottom of the CB is given by the empty Fe-3*d* states (almost flat bands at ~ -2 eV); the same feature is found in B3LYP, but in the HF the bottom of the CB is a band with larger dispersion, which has Fe-4*s* character. This behavior is typical of oxides with partially filled *d* orbitals: the self-interaction correction (introduced by the HF exchange) is larger the greater the localization of the states. In this case Fe-3*d* are much more localized than Fe-4*s*; on increasing the HF component the empty Fe-3*d* is destabilized with respect to the Fe-4*s*, until the order of their energies swaps. Similar behavior has already been observed in FeO .³¹

Using a convenient plane through the material that contains both types of cations as well as oxygen atoms, we have plotted in Fig. 4 the contour lines (a) of the charge density and (b) of the difference between this density and the superposition of the charge densities of the formal ions Fe^{3+} , Sb^{5+} , O^{2-} , which were calculated for each isolated ion using the same basis set as in the solid. The deviation from the ideal ionic charge density is more extensive for Sb than for Fe, suggesting a higher degree of covalence in the Sb-O than in the Fe-O interaction. A Mulliken analysis of the charge distribution yields charges of +2.26, +3.18, and -1.36 for Fe, Sb, and O, respectively, and higher overlap populations for Sb-O than for Fe-O pairs. The ionicity of the system increases with the amount of HF exchange included in

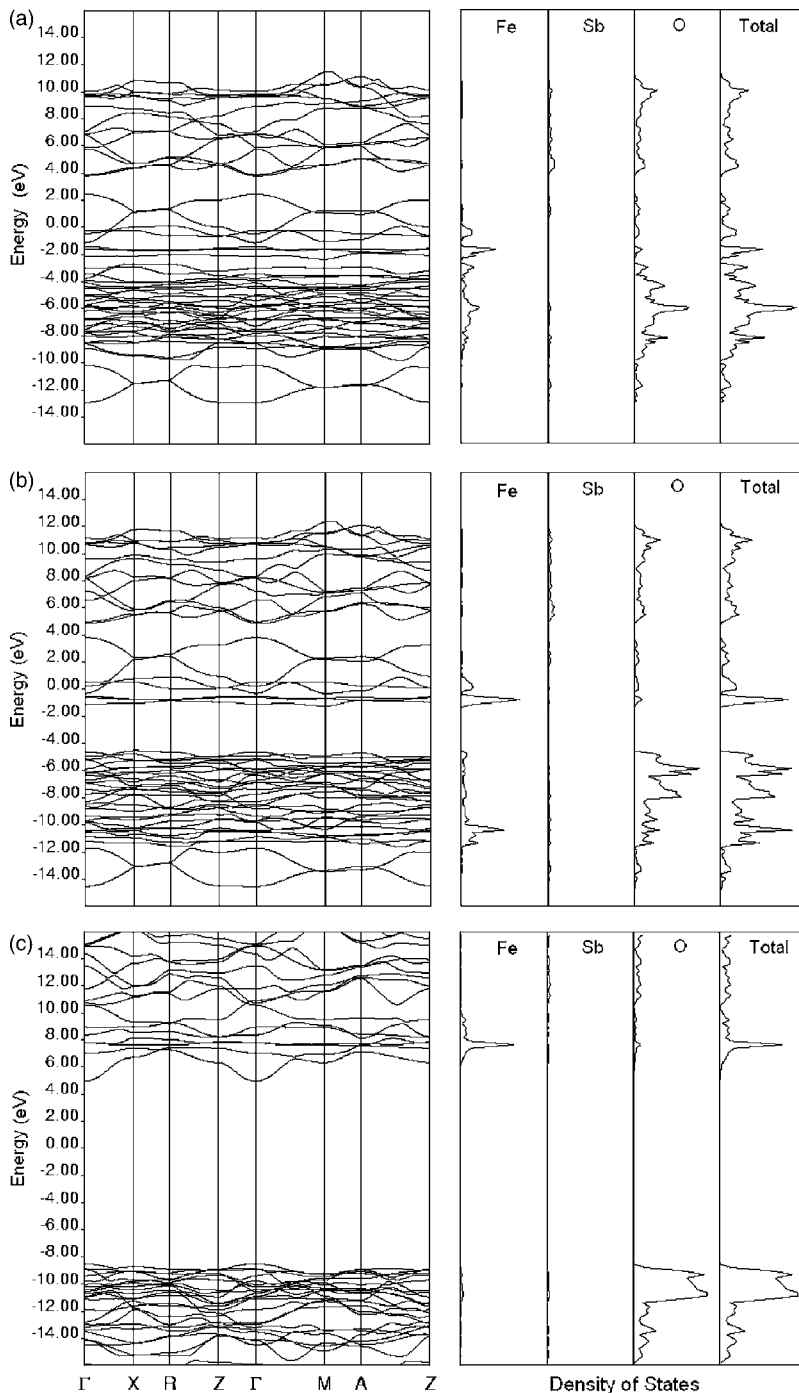


FIG. 3. Band structure, total, and projected density of states obtained using all-electron calculations with localized basis sets in (a) the GGA (BLYP) approximation, (b) the hybrid functional B3LYP, and (c) the Hartree-Fock method.

the calculation (Table II), with the charge and spin populations at their highest values and the overlap population at the lowest value at the HF limit.

Figure 5(a) shows a well-localized spin density on the Fe atoms, with antiferromagnetic order in the “zigzag” planes perpendicular to the c axis. As we have discussed in a previous work,⁷ because of the alternation of the Fe and Sb cations along the c axis, these magnetic planes are separated from each other by nonmagnetic Sb–O layers, giving rise to the experimentally observed³ two-dimensional magnetic behavior of FeSbO_4 . Figure 5 shows that the AFM correlation extends through the magnetic planes via a superexchange mechanism involving the oxygen atoms, even though the Fe–

O–Fe angle of $\sim 128^\circ$ is not particularly close to the 180° configuration which is the most favorable angle for superexchange coupling. Figure 5(b) shows details of the spin density around one of these O atoms connecting two Fe ions, with clear negative and positive regions pointing to the Fe atoms with negative and positive spin density, respectively. The inclusion of the Hartree-Fock exchange leads to a more localized spin density around each iron ion, increasing the spin population (see Table II) and at the same time weakening the superexchange interaction. The spin population, or the number of unpaired electrons, is expected to be 5 for Fe^{3+} in the high-spin $S=5/2$ state, which corresponds to a magnetic moment $2[S(S+1)]^{1/2}=5.93\mu_B$ (the experimental³²

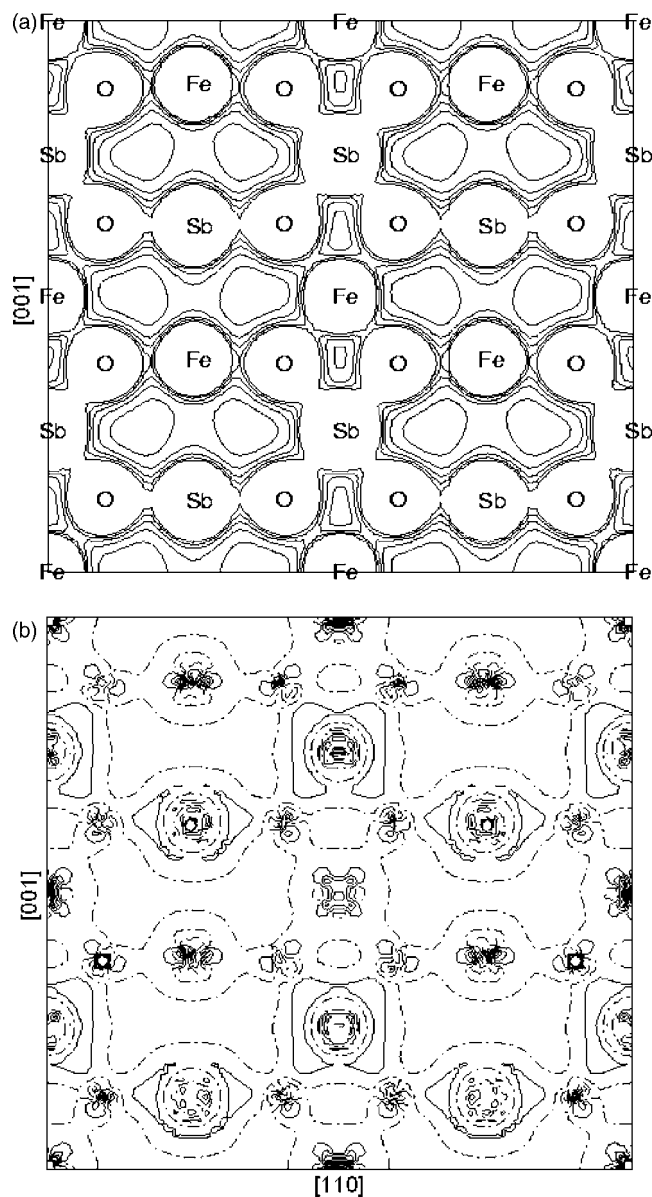


FIG. 4. (a) Charge density for the antiferromagnetic state calculated using the B3LYP functional, (b) difference charge density (free ion densities subtracted). Continuous, dashed and dotted-dashed lines correspond to positive, negative, and zero values of the plotted function. Contour lines are drawn from -0.10 to 0.10 at $0.02 e/\text{\AA}^3$ intervals in plot (a) and from -0.06 to 0.06 at $0.02 e/\text{\AA}^3$ intervals in plot (b).

magnetic moment of Fe ions in FeSbO_4 is $6.0 \pm 0.1 \mu_B$). The Fe spin population is therefore underestimated in all our calculations, which is the result of both the approximations involved in the methods, and of the Mulliken scheme for population analysis. The spin density shows no feature on the Sb ions, and the Mulliken analysis confirms the absence of net spin polarization on Sb.

Table III gives the energy difference between the antiferromagnetic and ferromagnetic phases and the corresponding magnetic coupling constants, obtained with the GGA, B3LYP, and HF functionals. All the values are negative, indicating the preference for AFM coupling, in agreement with

TABLE II. Mulliken population analysis of the antiferromagnetic solutions obtained by the three methods (GGA, B3LYP, and HF). Symbols q , q_b , and $\Delta q_{\alpha-\beta}$ refer to charge, overlap, and spin populations, respectively, and all values are given in electrons.

	GGA	B3LYP	HF
$q(\text{Fe})$	+2.10	+2.26	+2.64
$q(\text{Sb})$	+3.10	+3.18	+3.50
$q(\text{O})$	-1.30	-1.36	-1.54
$q_b(\text{Fe-O})$	0.04	0.03	0.01
$q_b(\text{Sb-O})$	0.16	0.16	0.14
$ \Delta q_{\alpha-\beta} (\text{Fe})$	3.91	4.30	4.78

the experimental evidence. Assuming that each Fe is coupled to four other Fe atoms, the experimental value of -25 K was calculated by Berry and co-workers^{32,33} from the Curie-Weiss temperature (580 K) obtained by measurements of susceptibility versus temperature. In agreement with other DFT studies of magnetic materials,^{13,34} the GGA calculations overestimate the magnitude of the coupling, in this case by a factor of 2.4. The HF method, on the other hand, tends to localize the spin density on Fe too much, hence reducing the effectiveness of the superexchange mechanism, and yielding a very weak coupling (-4 K). B3LYP yields a slightly underestimated but acceptable value (-21 K) of the magnetic coupling. Notably, the deviation from the experimental value of the superexchange constant is opposite to that found in other magnetic oxides, including MnO (B3LYP, -19.6 K, experiment; -11 K) and NiO (B3LYP, -249 K; experiment, -230 K).¹³

B. Plane-wave calculations

Figure 6 shows the variation of the cell parameters, the Fe spin, and the magnetic coupling with the parameter U_{eff} in the GGA+U approach, where the horizontal solid lines represent the experimental values. The scale used in each plot is chosen to show the whole range of variation in each case, but it should be noted that the relative deviations from the experimental values are very different from one plot to the other. The volume of the cell is slightly overestimated for all values of U_{eff} considered here, with a maximum deviation of $+3.1\%$ at $U_{\text{eff}}=2$ eV, and it seems that higher values of U_{eff} are needed to match the experimental volume. The c/a ratio is only slightly overestimated for all values of $U_{\text{eff}} < 8$ eV; where the maximum deviation ($+0.4\%$) occurs at the GGA limit.

The integral of the spin density within a sphere (radius 1.30\AA) around Fe can be used to evaluate the number of unpaired electrons on the iron d levels, which increases from 3.8 for $U_{\text{eff}}=0$ (GGA limit) to 4.7 for $U_{\text{eff}}=9$ eV. The number does not reach the value of five unpaired electrons that would be expected for high-spin Fe^{3+} according to experimental results,³² but it is reasonably close considering the approximations of this method of calculation. The electronic localization on the metal ion in GGA+U method correlates with the value chosen for U_{eff} , so it is not surprising that the

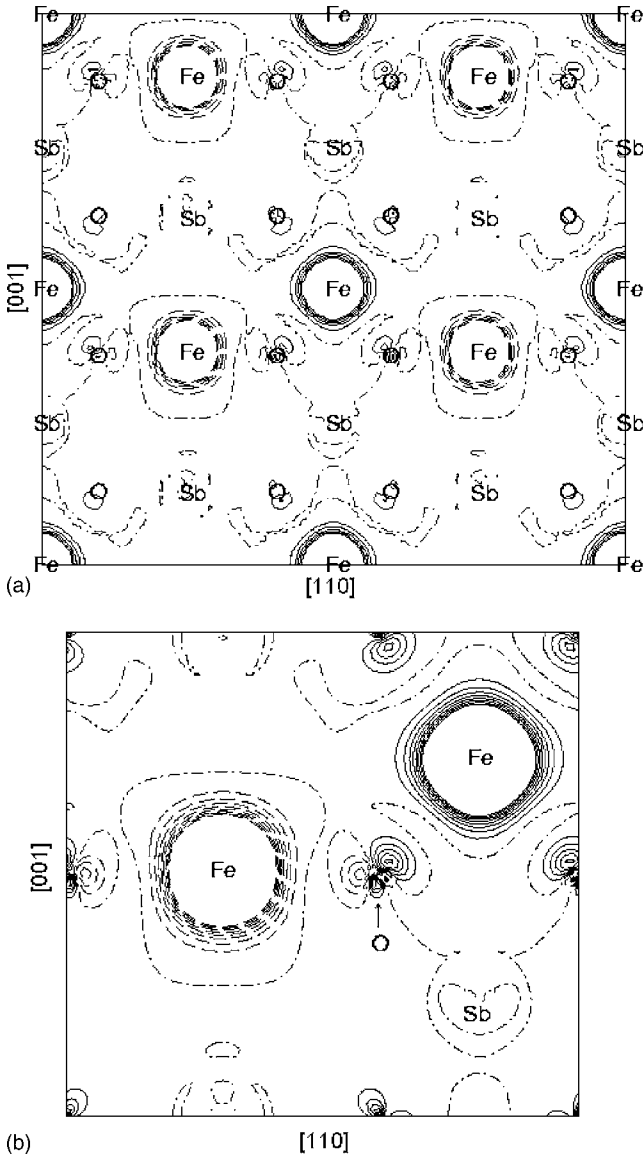


FIG. 5. (a) Spin density for the antiferromagnetic state calculated using the B3LYP functional and (b) magnification of the spin density around one O ion between two Fe. Continuous, dashed, and dotted-dashed lines correspond to positive, negative, and zero values of the plotted function. Contour lines are drawn from -0.10 to 0.10 at $0.02 e/\text{\AA}^3$ intervals in plot (a) and from -0.08 to 0.08 at $0.01 e/\text{\AA}^3$ intervals in plot (b).

TABLE III. Energy differences (in eV) between the antiferromagnetic and ferromagnetic phases and the corresponding magnetic coupling constants J (in kelvin).

Method	ΔE_{AFM-FM} (eV)	J (K)
GGA	-0.519	-60
B3LYP	-0.184	-21
HF	-0.034	-4
Experimental		-25

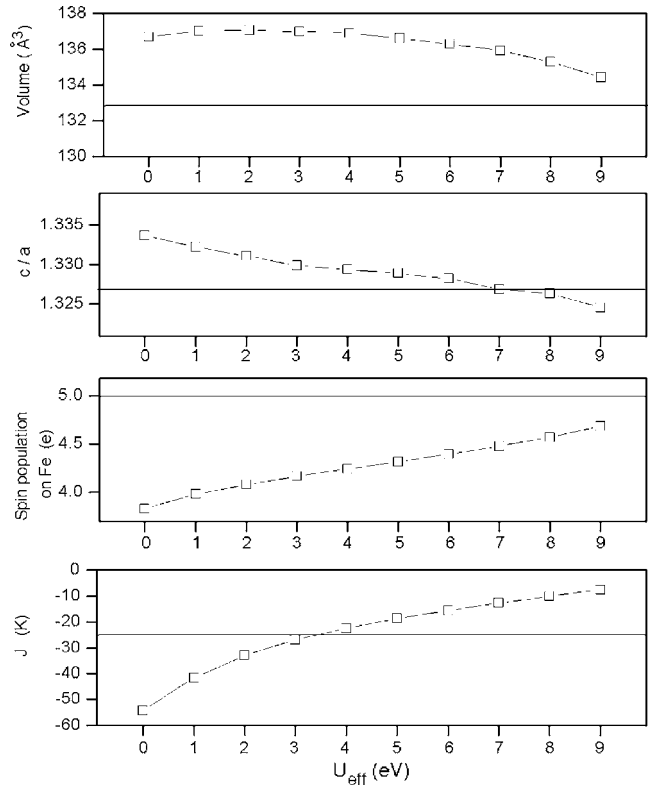


FIG. 6. Effect of the U_{eff} parameter on the calculated properties of FeSbO_4 . Horizontal lines represent experimental values (structure, Ref. 5; magnetic properties, Ref. 32).

spin density integration within a fixed sphere increases with this parameter.

Finally, the magnetic coupling constant exhibits a dramatic dependence on the U_{eff} parameter. At the GGA limit, the coupling strength of -54 K overestimates experiment. The difference from the value of -60 K obtained at the GGA (BLYP) level in the last subsection is relatively small and derives from the use of different functionals and types of basis sets. The coupling strength rapidly decreases with the U_{eff} parameter, as the spin localization on Fe increases and the superexchange interaction becomes less efficient. No significant change of the Fe–O–Fe angle is associated with this variation, which excludes a strong structural magnetostriction in the material. For U_{eff} between 3 and 4 eV, the calculated coupling is very close to the experimental value of -25 K. For $U_{eff}=4$ eV, the magnetic coupling $J=-22$ K is also close to the B3LYP value (-21 K), and for higher U_{eff} values, the J values decrease ($J=-7.5$ K for $U_{eff}=9$) and almost reach the HF value ($J=-4$ K) reported above. Here the analogy between the roles of the HF exchange in hybrid functionals and the DFT+U correction is close, suggesting a clear correspondence between the value of the HF exchange fraction in one method and the U_{eff} parameter in the other.

Considering the above results, we will use the magnetic coupling to select a convenient U_{eff} parameter value, as the structural properties are not as sensitive to this parameter. A value of 4 eV gives rise to a coupling strength that is close to experiment and to the B3LYP result, and still yields reason-

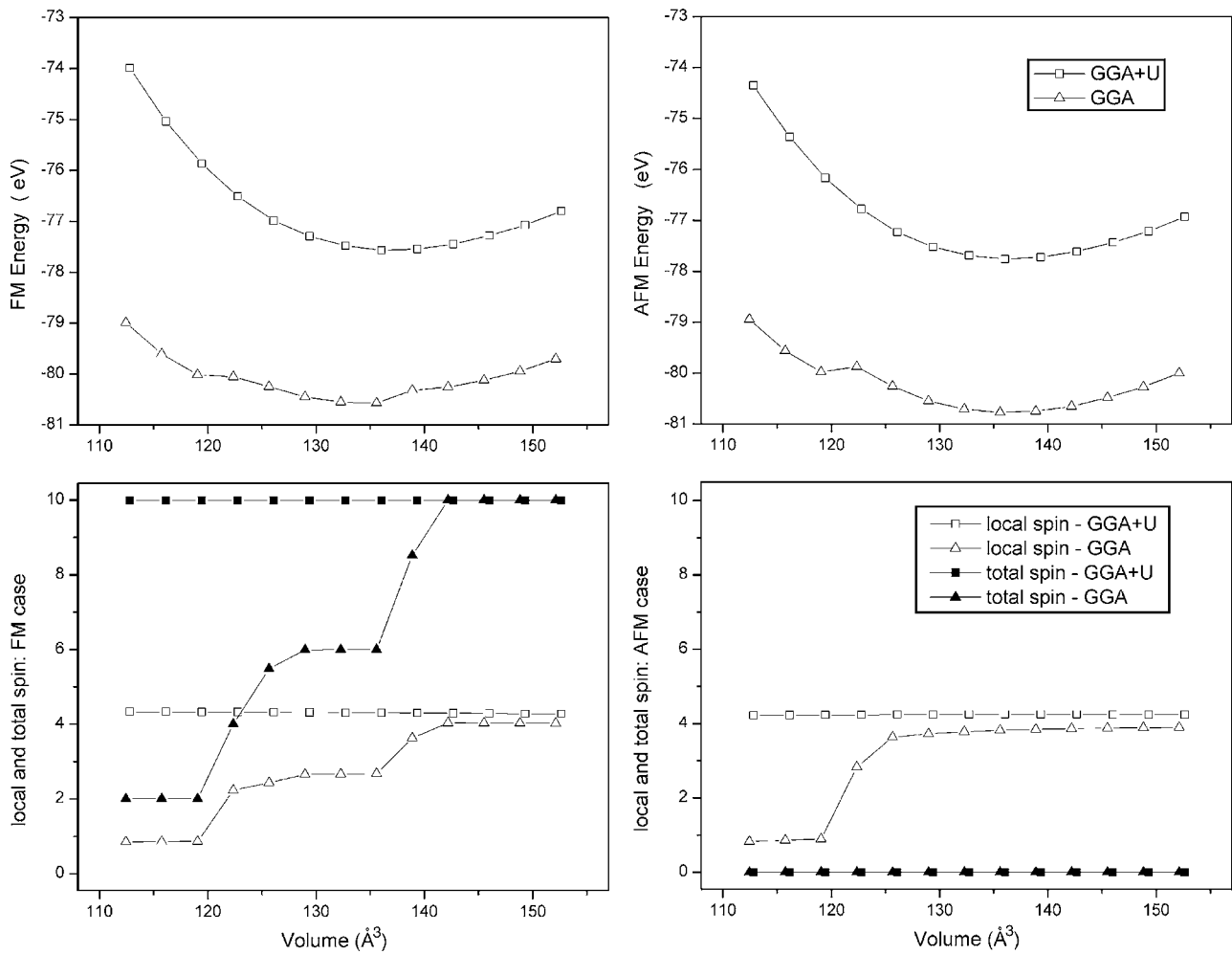


FIG. 7. Total energy and number of unpaired electrons as functions of the cell volume. Results for the ferromagnetic (FM) cell are shown on the left, and for the antiferromagnetic (AFM) cell on the right.

able cell parameters (see Table I). It is worth noting that the same value of $U_{eff}=4$ eV has been found to lead to optimal agreement between calculation and experiment for a range of physical properties of hematite (α - Fe_2O_3).^{35,36} Thus, from now on, all GGA+U results refer to those obtained using this value of U_{eff} , unless otherwise stated.

The variation of the total energy and the Fe spin with the cell volume is shown in Fig. 7, for GGA and GGA+U calculations of the FM and the AFM phases. In all cases the total spin was allowed to relax, and FM or AFM solutions were controlled by setting the initial spin populations around the Fe atoms. In the E - V curves obtained within the GGA there are clear kinks which are associated with Fe spin transitions from high spin (HS) to intermediate spin (IS) to low spin (LS) in the FM case, and from HS to LS in the AFM case. The HS-IS transition in the FM phase occurs at nearly zero external pressure, while transitions to LS occur at ~ 15 GPa in both FM and AFM phases. Although pressure-induced spin transitions can actually occur,³⁷⁻³⁹ transition pressures are typically much higher [e.g., ~ 50 GPa in Fe_2O_3 (hematite) Ref. 37 and EuFeO_3 , Ref. 38 and ~ 100 GPa in FeSiO_3 Ref. 39]. Rollmann *et al.* have recently found that the GGA approximation predicts a spin transition in hematite at

14 GPa, which is well below the experimental transition pressure. We therefore conclude that the spin transitions obtained in our GGA calculations of FeSbO_4 at relatively low pressures are most likely an artifact of the simulation method. The GGA+U technique corrects the problem, as can be seen in the figure, giving, for example, the correct total of ten unpaired electrons per cell (two Fe ions) in the FM solution for all cell volumes investigated here.

Total and site-projected DOS are shown in Fig. 8 from both GGA and GGA+U calculations. In agreement with the results of the all-electron calculations, the GGA band structure presents a very small gap (of around 0.2 eV). The GGA+U result shows a wider band gap of 1.6 eV. This value is lower than the B3LYP result, and although here the band gap increases with the U_{eff} parameter, it saturates and never reaches the large value for the gap obtained in the HF calculation (see Table IV). For example, increasing the U_{eff} parameter up to 9 eV, increases the band gap by less than 0.1 eV. Thus, in this case, the U_{eff} correction does not act in complete analogy with the incorporation of the HF exchange in the hybrid functional. This finding is not surprising because the GGA+U correction acts selectively on the metal d levels, shifting down the occupied d bands, and, once these orbitals are far from the gap region, the effect of the U_{eff}

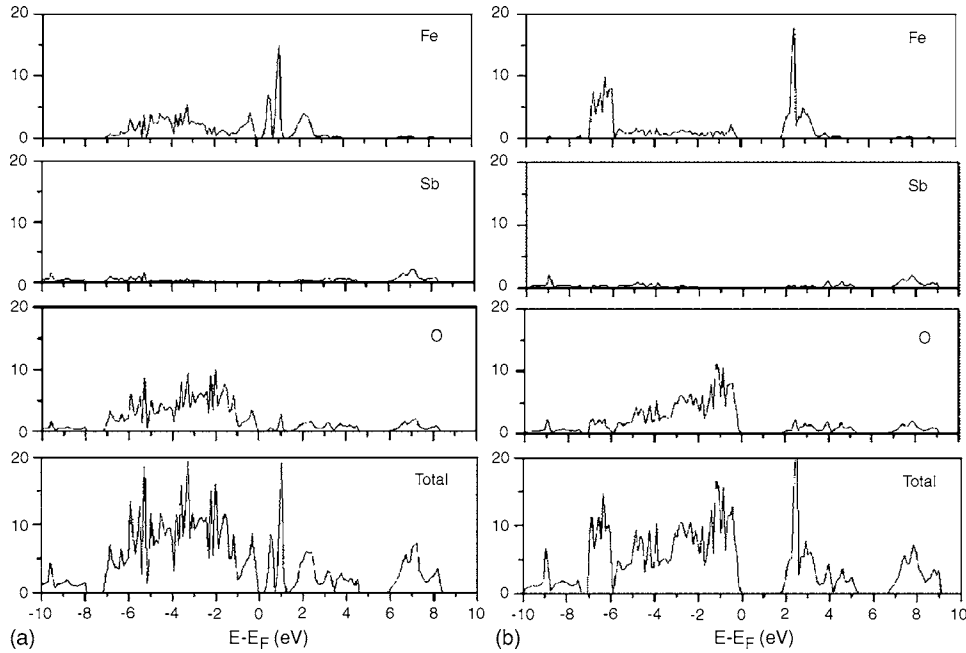


FIG. 8. Site-projected and total electronic DOS (states/eV) obtained for the antiferromagnetic phase using (a) GGA and (b) GGA+U ($U_{eff}=4$ eV).

correction on the width of the band gap is very small. In contrast, the inclusion of the HF exchange in a hybrid functional acts on each electronic state (including those on O and Sb) and produces a dramatic drop in the energy of the O- p states (Fig. 3), partly attributable to a stronger Madelung field resulting from a higher charge localization, and partly due to the self-interaction cancellation in O- p states. Hence, the band gap is likely to be underestimated by this GGA+U approach due to the overestimation of the O- p energy bands.

The partial DOS plots show that whereas in the GGA solution the top edge of the VB has a mixed Fe- d O- p character, in the GGA+U solution the top of the VB has almost only O- p character, just like the B3LYP calculations. In general, the relative positions of the total and site-projected DOS peaks are very similar for B3LYP and GGA+U.

IV. CONCLUSIONS

We have presented a computer modeling study of the electronic and magnetic properties of iron antimonate FeSbO_4 , showing the limitations of traditional (e.g., GGA) DFT formulations to treat this mixed-metal oxide and comparing the performance of two different approaches to surmount these difficulties: the use of hybrid functionals and the DFT+U method.

TABLE IV. Electronic band gap values (in eV) obtained for the antiferromagnetic solutions using different methods.

CRYSTAL	Band gap (eV)	VASP	Band gap (eV)
GGA (BLYP)	0.2	GGA (PW91)	0.2
B3LYP	3.0	GGA+U ($U_{eff}=4$ eV)	1.6
HF	12.8	GGA+U ($U_{eff}=9$ eV)	1.7

The strength of the magnetic coupling in the material is reasonably well predicted by a hybrid functional which incorporates 20% of Hartree-Fock exchange (B3LYP) and by the GGA+U calculation with $U_{eff}=4$ eV. The analysis of the spin density shows a clear superexchange mechanism for the propagation of the antiferromagnetic correlations in the crystal, and this mechanism lessens with the increase in the localization of the spin density that occurs after the inclusion of either the HF exchange or the U_{eff} correction. At the GGA level, the strength of the magnetic coupling is considerably overestimated, while at the HF level, or in the GGA+U method with high U_{eff} , the magnitude of the coupling is underestimated. The dramatic dependence of the magnetic coupling on the U_{eff} parameter in the GGA+U provides a simple method to select the value of this computational parameter for those systems where experimental measurements of magnetic susceptibilities are available. For FeSbO_4 , the value of $U_{eff}=4$ eV yields a good description of both magnetic and structural properties.

According to both B3LYP and GGA+U calculations, FeSbO_4 is a semiconductor material with an O- p -Fe- d band gap, i.e., of a charge transfer rather than a Mott-Hubbard character. The band gap and the relative positions of the bands are affected in similar ways by the inclusion of 20% Hartree-Fock exchange and by the GGA+U correction with $U_{eff}=4$ eV. In particular, the occupied Fe-3 d levels shift down in the valence band region for both methods, in comparison with the GGA solutions. However, increasing the HF exchange up to 100% and using higher values of U_{eff} do not have equivalent effects on the band structure, due to the local character of the GGA+U correction.

Although there are no experimental studies on the details of the electronic structure of iron antimonates for comparison with our results, the consistency between our B3LYP and GGA+U results, and the reported success of these methods

in the description of other transition metal oxides, give us confidence in the validity of our results. Experimental verification, for example by photoemission experiments or other spectroscopic measurements, would, of course, be of considerable interest to confirm our predictions. The present description of the bulk electronic structure now provides a solid basis for the investigation of the electronic properties of the FeSbO₄ surfaces and oxygen vacancies, which play a crucial

role in the catalytic applications of this material.

ACKNOWLEDGMENTS

We thank EPSRC for financial support under Grant No. GR/S01986/01, and the EPSRC-funded Materials Chemistry Consortium for access to HPCx.

*Email address: r.grau-crespo@mail.cryst.bbk.ac.uk

- ¹G. W. Keulks and M. Y. Lo, *J. Phys. Chem.* **90**, 4768 (1986).
- ²T. S. Zhang and P. Hing, *J. Mater. Sci.* **10**, 509 (1999).
- ³X. Obradors, J. Bassas, J. Rodriguez, J. Pannetier, A. Labarta, J. Tejada, and F. J. Berry, *J. Phys.: Condens. Matter* **2**, 6801 (1990).
- ⁴M. T. Causa, M. Tovar, X. Obradors, A. Labarta, and J. Tejada, *Phys. Rev. B* **44**, 4455 (1991).
- ⁵P. Berlepsch, T. Armbruster, J. Brugger, A. J. Criddle, and S. Graeser, *Chem. Mater.* **67**, 31 (2003).
- ⁶R. Grau-Crespo, N. H. de Leeuw, and C. R. A. Catlow, *Chem. Mater.* **16**, 1954 (2004).
- ⁷R. Grau-Crespo, N. H. de Leeuw, and C. R. A. Catlow, *J. Mater. Chem.* **13**, 2848 (2003).
- ⁸G. Kresse and J. Furthmuller, *Comput. Mater. Sci.* **6**, 15 (1996).
- ⁹G. Kresse and J. Furthmuller, *Phys. Rev. B* **54**, 11169 (1996).
- ¹⁰G. Kresse and J. Hafner, *Phys. Rev. B* **48**, 13115 (1993).
- ¹¹G. Kresse and J. Hafner, *J. Phys.: Condens. Matter* **6**, 8245 (1994).
- ¹²V. R. Saunders, R. Dovesi, C. Roetti, R. Orlando, C. M. Zicovich-Wilson, N. M. Harrison, K. Doll, B. Civalleri, I. Bush, P. D'Arco, and M. Llunel, *CRYSTAL2003 User's Manual* (University of Torino, Torino, 2003).
- ¹³F. Corà, M. Alfredsson, G. Mallia, D. S. Middlemiss, W. C. Mackrodt, R. Dovesi, and R. Orlando, in *Structure and Bonding* (Springer-Verlag, Berlin Heidelberg, 2004), Vol. 113, p. 171.
- ¹⁴A. D. Becke, *Phys. Rev. A* **38**, 3098 (1988).
- ¹⁵C. Lee, W. Yang, and R. G. Parr, *Phys. Rev. B* **37**, 785 (1988).
- ¹⁶M. Catti, G. Valerio, and R. Dovesi, *Phys. Rev. B* **51**, 7441 (1995).
- ¹⁷M. D. Towler, <http://www.tcm.phy.cam.ac.uk/~mdt26/crystal.html>.
- ¹⁸V. I. Anisimov, J. Zaanen, and O. K. Andersen, *Phys. Rev. B* **44**, 943 (1991).
- ¹⁹A. Rohrbach, J. Hafner, and G. Kresse, *J. Phys.: Condens. Matter* **15**, 979 (2003).
- ²⁰A. I. Liechtenstein, V. I. Anisimov, and J. Zaanen, *Phys. Rev. B* **52**, R5467 (1995).
- ²¹S. L. Dudarev, G. A. Botton, S. Y. Savrasov, C. J. Humphreys, and A. P. Sutton, *Phys. Rev. B* **57**, 1505 (1998).
- ²²I. V. Solovyev, P. H. Dederichs, and V. I. Anisimov, *Phys. Rev. B* **50**, 16861 (1994).
- ²³J. P. Perdew and A. Zunger, *Phys. Rev. B* **23**, 5048 (1981).
- ²⁴S. H. Vosko, L. Wilk, and M. Nusair, *Can. J. Phys.* **58**, 1200 (1980).
- ²⁵J. P. Perdew, J. A. Chevary, S. H. Vosko, K. A. Jackson, M. R. Pederson, D. J. Singh, and C. Fiolhais, *Phys. Rev. B* **46**, 6671 (1992).
- ²⁶P. E. Blochl, *Phys. Rev. B* **50**, 17953 (1994).
- ²⁷G. Kresse and D. Joubert, *Phys. Rev. B* **59**, 1758 (1999).
- ²⁸F. D. Murnaghan, *Proc. Natl. Acad. Sci. U.S.A.* **30**, 244 (1944).
- ²⁹G. P. Francis and M. C. Payne, *J. Phys.: Condens. Matter* **2**, 4395 (1990).
- ³⁰J. M. M. Millet, I. C. Marcu, and J. M. Herrmann, *J. Mol. Catal. A: Chem.* **226**, 111 (2005).
- ³¹M. Alfredsson, G. D. Price, C. R. A. Catlow, S. C. Parker, R. Orlando, and J. P. Brodholt, *Phys. Rev. B* **70**, 165111 (2004).
- ³²F. J. Berry, M. I. Sarson, A. Labarta, X. Obradors, R. Rodriguez, and J. Tejada, *J. Solid State Chem.* **71**, 582 (1987).
- ³³A. Labarta, M. Sarson, X. Obradors, F. Berry, R. Rodriguez, and J. Tejada, *IEEE Trans. Magn.* **23**, 2311 (1987).
- ³⁴D. Dai, M.-H. Whangbo, H.-J. Koo, X. Rocquefelte, S. Jobic, and A. Villesuzanne, *Inorg. Chem.* **44**, 2407 (2005).
- ³⁵A. Rohrbach, J. Hafner, and G. Kresse, *Phys. Rev. B* **70**, 125426 (2004).
- ³⁶G. Rollmann, A. Rohrbach, P. Entel, and J. Hafner, *Phys. Rev. B* **69**, 165107 (2004).
- ³⁷J. Badro, G. Fiquet, V. V. Struzhkin, M. Somayazulu, H. K. Mao, G. Shen, and T. Le Bihan, *Phys. Rev. Lett.* **89**, 205504 (2002).
- ³⁸W. M. Xu, M. P. Pasternak, G. K. Rozenberg, and R. D. Taylor, *Hyperfine Interact.* **141**, 243 (2002).
- ³⁹J. Li, V. V. Struzhkin, H. K. Mao, J. F. Shu, R. J. Hemley, Y. W. Fei, B. Mysen, P. Dera, V. Prakapenka, and G. Y. Shen, *Proc. Natl. Acad. Sci. U.S.A.* **101**, 14027 (2004).